WebCam for Interactive Multispectral Measurements

Hans Brettel, Jon Yngve Hardeberg* and Francis Schmitt

Signal and Image Processing Department
École Nationale Supérieure des Télécommunications, Paris, France
*Conexant Systems, Imaging Software Team, Redmond, Washington, U.S.A.

A fully electronic multispectral imaging system is described which provides interactive access to reflectance spectra at any position on the target. The user typically first selects the reference 'white' position by means of the mouse cursor, and then interactively examines reflectance spectra, CIE XYZ tristimulus values, or CIELab data for any region of interest on the target. The key elements of the system are an electronically controlled liquid crystal tunable filter, a monochrome digital camera, and modular software components which make the system accessible through a Web server.

1 Introduction

Highly accurate cross-media colour reproduction often requires spectrophotometric measurements of imaging targets. In a conventional laboratory setup such measurements are done by manual or semi-automatic operation of a specific optical instrument, such as a spectroradiometer. Each individual measurement typically requires mechanical repositioning of the target with respect to the actual measuring spot of the instrument, and spatial resolution, speed, and interactivity are severely limited.

Electronic cameras, on the other hand, are fast and provide high spatial resolution but they are generally limited to a given set of three spectral bands only. With regard to the growing interest in the development and application of multispectral image acquisition and analysis [1, 2, 3, 4, 5], several solutions to overcome the three-band-only limitation were proposed. They are usually based on a combination of a monochrome or trichrome digital camera with a suitable set of additional filters [6, 7]. In a typical setup, a given number of interference filters is mounted on a filter wheel in front of a monochrome digital camera. The number of readily available spectral channels is therefore limited, and mechanical filter switching is required.

Here we report in Section 2 a system for multispectral image acquisition and analysis which uses an electronically tunable spectral filter and a monochrome digital CCD camera of photometric quality. The filter and the camera are controlled through Java servlets which allow for interactive operation of the multispectral camera across the Web. We also present, in Section 3, two interesting applications, a *colorimetric WebCam* that implements the spectral sensitivity functions of the CIE 1931 Standard Colorimetric Observer [8, 9], and a camera that provides output signals required for a colorimetrically correct imaging chain using an ITU-R BT.709 [10] or sRGB [11] compatible display device.

2 Multispectral Image Acquisition

Each pixel of a multispectral image contains information about the spectral reflectance of the imaged scene. Multispectral images carry information about a number of spectral bands: from three components per pixel for RGB colour images to several hundreds of bands for hyperspectral images.

Multispectral imaging is relevant to several domains of application, such as remote sensing [12], astronomy [13], medical imaging, analysis of museological objects [3, 14], cosmetics, medicine [15], high-accuracy colour printing [4, 16], or computer graphics [17].

In this section we present the different elements constituing a multispectral camera system called *SpectraCam* that we have set-up in our laboratory.

2.1 Electronically Tunable Filter

The key element of our system is a liquid crystal tunable filter (LCTF) which allows for continuous tuning of its peak transmission wavelength over the full range of the visible spectrum. The spectral transmission profile is similar to a gaussian function, and the LCTF is operated completely electronically, without any moving parts.

The optical principle of this type of spectral filter was introduced by Bernard Lyot in 1933, when he suggested to use a series of birefringent plates between polarizers in order to set up a monochromatic filter [18]. Birefringent materials have slightly different refractive indices n_o and n_e for two orthogonal planes of polarization, respectively known as the planes of the ordinary and the extraordinary rays. Since the refraction index n of a material is the ratio of the speed of light in vacuum c to the speed of light in that material $c_{material}$

$$n = c/c_{material}, \tag{1}$$

an incident lightwave with its electric field component in the polarization plane of the ordinary ray travels through the birefringent material at a different speed than its orthogonally polarized counterpart. The difference $\Delta n = n_o - n_e$ leads to a phase lag between the ordinary and extraordinary rays. For a birefringent plate of thickness d_k, the phase lag δ between the two rays is

$$\delta = 2\pi\ d_k \Delta n/\lambda \tag{2}$$

where λ is the wavelength in vacuum. A single stage of a Lyot filter consists of such a retarder plate between parallel linear polarizers; the plane of polarization forms an angle of $45°$ with the n_o and n_e directions of the birefringent plate. This results in a circularly polarized wave propagating through the plate, and the angle of polarization at the end of the plate is given by δ. For a wave of amplitude A, the second polarizer lets pass only the parallel component $A_{||}$:

$$A_{||} = A\cos(\delta). \tag{3}$$

Since filter transmittance is defined as a ratio of light *intensities* I rather than amplitudes A, and

$$I \propto A^2, \tag{4}$$

we conclude from equations (2) to (4) that the transmittance $\tau_k(\lambda)$ of a single Lyot stage of thickness d_k can be expressed as

$$\tau_k(\lambda) = \cos^2(2\pi\ d_k \Delta n/\lambda) \tag{5}$$

The transmittance function (5) of a single stage shows a series of minima and maxima (see Figure 1), and more selective filters consist of a series of such stages where the thicknesses d_k of the birefringent plates decreases progressively. In a Lyot filter, the thickness d_k of any individual stage is always a multiple of the thickness d_1 of the thinnest plate:

$$d_k = k\ d_1 \tag{6}$$

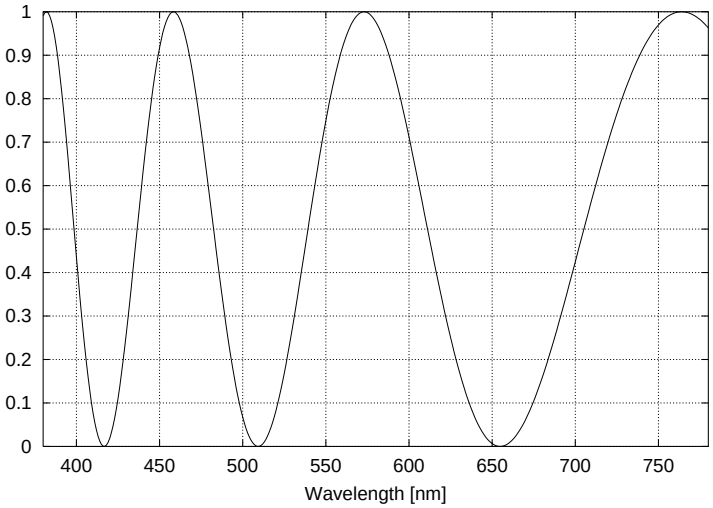

Figure 1: Theoretical spectral transmission function $\tau_k(\lambda)$ of a single stage of a Lyot filter.

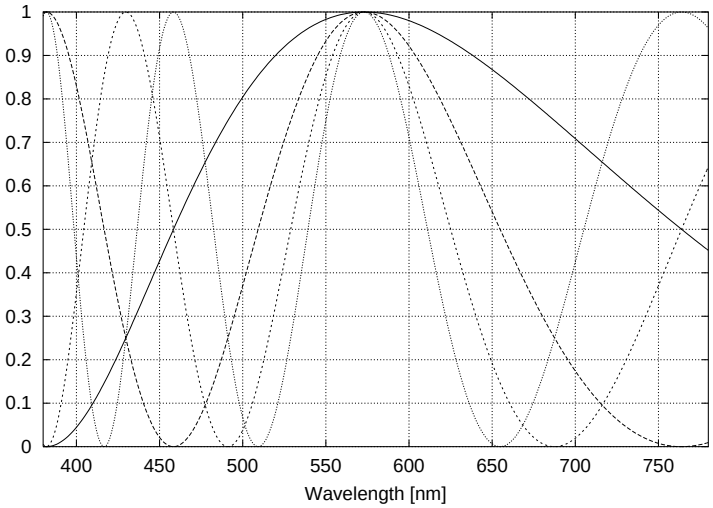

Figure 2: Theoretical spectral transmission functions $\tau_1(\lambda), \tau_2(\lambda), \tau_3(\lambda), \tau_4(\lambda)$ of each element of a 4-stage Lyot filter.

In a *tunable* spectral filter of the Lyot type, there is a liquid crystal cell added to each retarder plate in order to allow for an additional phase shift under control of an electric signal [19]. The spectral width of the passband of such a filter is primarily determined by the thickest retarder plate whereas the other stages attenuate all but one of the multiple transmittance maxima of the thickest plate.

A theoretical model of this successive selection process is illustrated in Figures 1 to 3 for a 4-stage Lyot filter. The spectral transmittance factors of the individual stages shown in Figure 2 are:

$$\tau_k(\lambda) = \cos^2(2\pi\ k\ d_1 \Delta n/\lambda), \quad k = 1, 2, 3, 4 \tag{7}$$

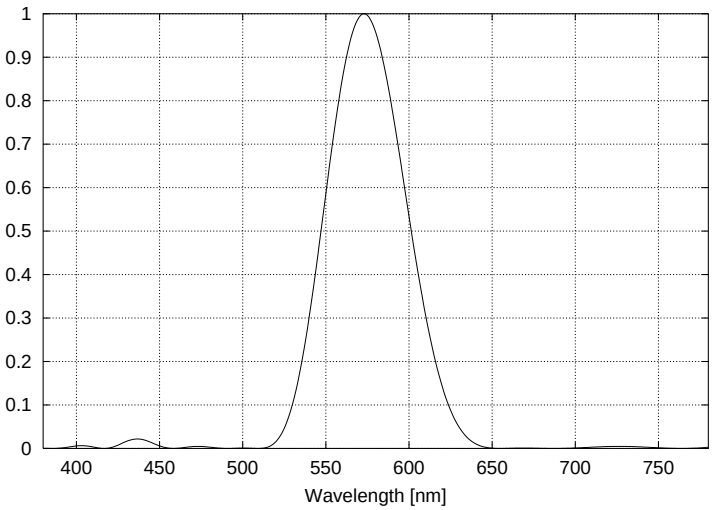

Figure 3: Theoretical spectral transmission function of a 4-stage Lyot filter. The plotted curve shows the product of the 4 transmission functions $[\tau_1(\lambda)\ \tau_2(\lambda)\tau_3(\lambda)\ \tau_4(\lambda)]$.

and the resulting transmission function of the 4-stage Lyot filter, shown in Figure 3, is given by the product

$$\tau_1(\lambda)\ \tau_2(\lambda)\ \tau_3(\lambda)\ \tau_4(\lambda) = \prod_{k=1}^{4} \cos^2(2\pi\ k\ d_1 \Delta n/\lambda) \tag{8}$$

A value of $d_1\Delta n = 286$ nm was arbitrarily chosen in order to simulate a transmittance profile resembling one of those of the real filter shown in Figure 4.

We use a liquid crystal tunable filter (LCTF) VariSpec Model VIS2 (Cambridge Research & Instrumentation, Inc., Boston, MA) with a nominal bandwidth of 30 nm and a nominal accuracy of the selected peak wavelength of 4 nm. This allows to select about 80 significantly different tuning positions in the range from 400 nm to 720 nm.

Figure 4 shows the measured transmittance curves of the LCTF of our *SpectraCam* system for nine peak wavelength positions. These curves reveal the desired gaussian like areas of high sensitivity, but they also show minor sidelobes which could be expected from the theoretical analysis presented above (cf. Figure 3). The biggest sidelobe near 700 nm belongs to the filter profile which peaks near 400 nm. The four smaller sidelobes in the range from 400 nm to 480 nm successively belong to the filter profiles peaking near 605, 650, 685, and 720 nm, respectively. These artifacts have to be carefully compensated for in applications requiring spectral or colorimetric measurements of high accuracy.

2.2 Digital Camera

Behind the tunable filter, a monochrome digital camera serves for image capture. We use a PCO SensiCam Model 370 KL camera with 1280 x 1024 pixels on a progressive scan CCD image sensor (PCO Computer Optics, 93309 Kelheim, Germany). The CCD sensor is Peltier cooled to a temperature of -12 centigrade for low noise image acquisition and the output signal is 12 bit AD converted. The CCD camera features an electronic shutter and the exposure time can be varied in 1 msec steps

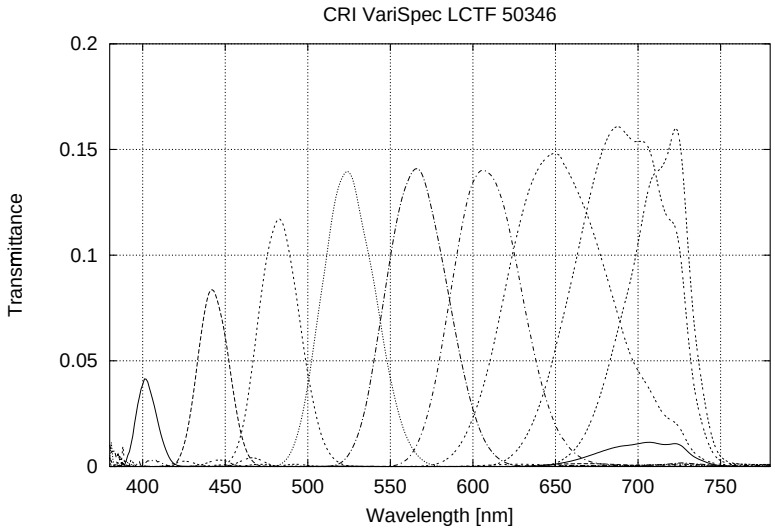

Figure 4: Spectral transmittance curves of the liquid crystal tunable filter VariSpec Model VIS2 (SN 50 346) for initially unpolarized light; measured with a Minolta spectroradiometer CS-1000.

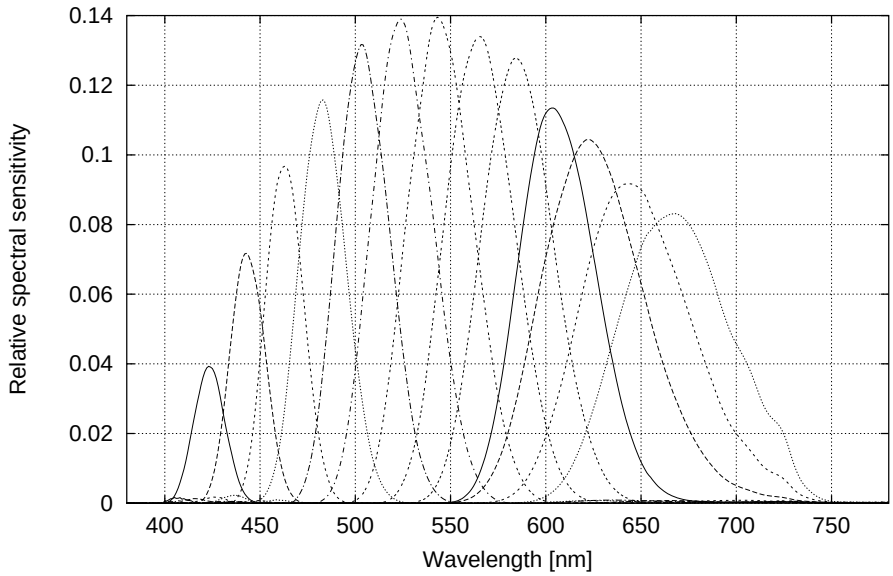

Figure 5: Effective spectral sensitivity functions of the most commonly used 13 channels of our SpectraCam system. These curves were obtained by multiplying the spectral transmittance functions of the liquid crystal tunable filter VariSpec Model VIS2 (SN 50 346) with the spectral sensitivity function of the PCO Sensicam Model 370 KL monochrome camera.

over the range from 1 msec to 1000 sec. The linearly 12 bit encoded pixel data are transferred by a high speed serial link to a specialized PCI interface (PCO Interface Board 520KP).

The spectral sensitivity of the image sensor (Sony ICX085AL) has its maximum near 510 nm

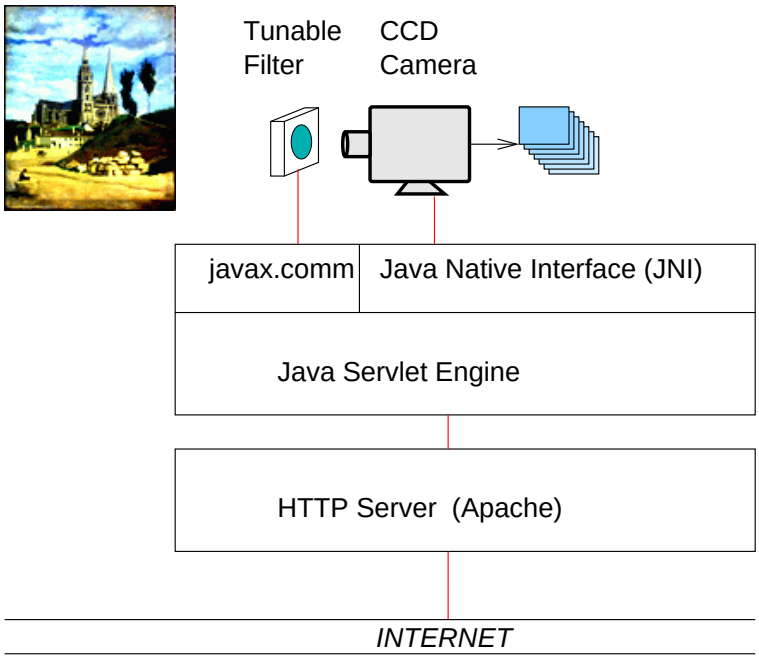

Figure 6: Schematic overview of our SpectraCam *system. A monochrome CCD camera is used for image acquisition through a tunable spectral bandpass filter. The image stack on the right of the camera symbolically represents an example in which the image was captured at seven different peak wavelengths of the tunable filter. Both, the tunable filter and the CCD camera are controlled by Java servlets which are accessible via Internet through simple HTTP requests.*

and shows about 10 percent variation in the wavelength range from 450 nm to 580 nm. Figure 5 shows the effective spectral sensitivity functions of our multispectral WebCam system for the most commonly used 13 channels. These curves were obtained by multiplying the spectral transmittance functions of the liquid crystal tunable filter with the spectral sensitivity function of the monochrome digital camera.

2.3 Network Link

In our system, the tunable filter and the CCD camera are both controlled by a PC-type computer which is linked via Ethernet to the campus-wide Local Area Network (LAN) and the Internet as shown in Figure 6.

In order to allow for interactive use of this multispectral image acquisition system through the network, we developed a set of Java Servlets which provide access to the system through Hypertext Transfer Protocol (HTTP) requests.

The choice of the HyperText Transfer Protocol (HTTP) [20] as basis for client-server communication for our *SpectraCam*-system was obvious since the HTTP is used by all Web-browsers and Web-servers on the Internet. For the same reason, we further choose the HyperText Markup Language (HTML) [21] to deliver usage information and requested results from the *SpectraCam* server to the clients on the Internet.

The basic elements of user interaction are implemented through HTML 'form' actions and the standard Common Gateway Interface (CGI) mechanisms for client-server communication. Taken to-

gether, these design choices assure that the *SpectraCam* system is accessible from any Web browser.

On the server-side, we choose the Java Servlet API as standard for extending the basic Web server functionality with the *SpectraCam* specific services. Java servlets are commonly known as a versatile means to generate dynamic Web pages, for example by adding specific information concerning a particular e-business transaction. The major advantage of Java servlets for our application is, however, the possibility to make use of all the features that the Java environment provides on the server computer.

The specific native functions required for the operation of the digital CCD camera were called through the Java Native Interface (JNI) [22]. The liquid crystal tunable filter was controlled by means of the Java Communications API which contains support for RS232 serial ports [23], and the Jama package [24] was used for the linear algebra operations for multispectral data processing, including matrix inversion and singular value decomposition.

3 Colorimetric WebCam

For practical applications, it is interesting to implement specific types of spectral sensitivity functions on a multispectral WebCam.

In the CIE 1931 Standard Colorimetric System[8, 25], the colorimetric properties of a stimulus of any spectral power distribution $\varphi(\lambda)$ are described by a tristimulus vector $[X, Y, Z]^t$. The components of this vector, called tristimulus values, are obtained by numerical integration from the spectral power distribution $\varphi(\lambda)$ of the stimulus and three different spectral weighting functions $\bar{x}(\lambda), \bar{y}(\lambda), \bar{z}(\lambda)$ (see Figure 7) which take into account the colour-matching properties of the human observer[9]:

$$\begin{aligned} X &= k \int \bar{x}(\lambda)\, \varphi(\lambda)\, \mathrm{d}\lambda, \\ Y &= k \int \bar{y}(\lambda)\, \varphi(\lambda)\, \mathrm{d}\lambda, \\ Z &= k \int \bar{z}(\lambda)\, \varphi(\lambda)\, \mathrm{d}\lambda. \end{aligned} \tag{9}$$

In Eqs. (9), $\bar{x}(\lambda), \bar{y}(\lambda), \bar{z}(\lambda)$ are the CIE 1931 colour matching functions and k is a constant which determines the photometric unit. The luminance Y is obtained in photometric SI units (Système Internationale d'Unitées) if $k = K_m$ where K_m = 683 lumen per Watt. By using sampled versions instead of continuous spectral functions over the visible spectrum (360 nm - 780 nm), the integrals in Eqs. (9) turn into sums:

$$\begin{aligned} X &= k \sum_{\lambda_i = 360\,\mathrm{nm}}^{780\,\mathrm{nm}} \bar{x}_{\lambda_i}\, \varphi_{\lambda_i}, \\ Y &= k \sum_{\lambda_i = 360\,\mathrm{nm}}^{780\,\mathrm{nm}} \bar{y}_{\lambda_i}\, \varphi_{\lambda_i}, \\ Z &= k \sum_{\lambda_i = 360\,\mathrm{nm}}^{780\,\mathrm{nm}} \bar{z}_{\lambda_i}\, \varphi_{\lambda_i}, \end{aligned} \tag{10}$$

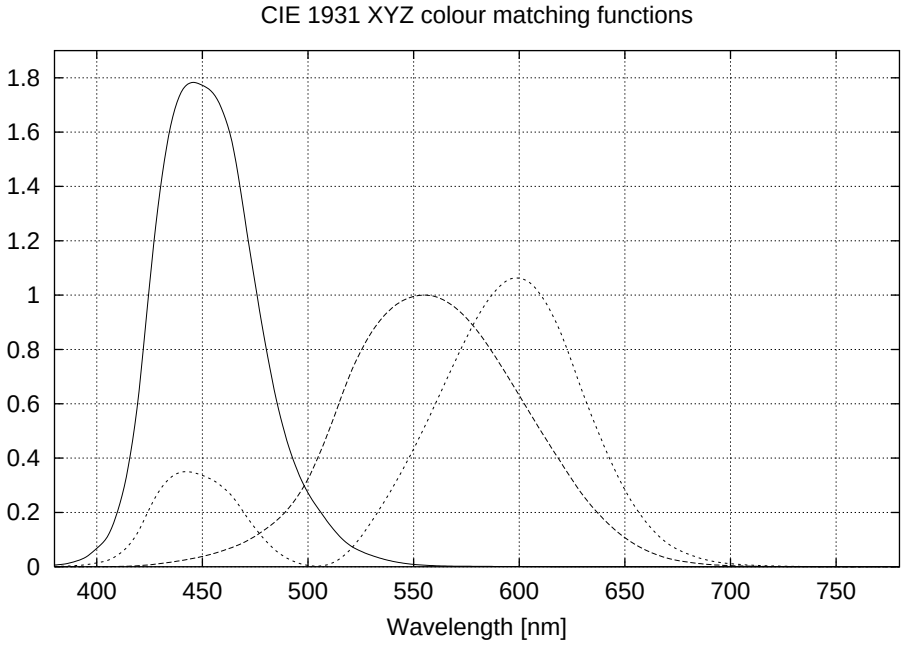

Figure 7: Colour matching functions of the CIE 1931 standard colorimetric observer in the XYZ-system.

which can be written in matrix notation:

$$\begin{bmatrix} X \\ Y \\ Z \end{bmatrix} = k \begin{bmatrix} \bar{x}_{\lambda_1} & \bar{x}_{\lambda_2} & \dots & \bar{x}_{\lambda_N} \\ \bar{y}_{\lambda_1} & \bar{y}_{\lambda_2} & \dots & \bar{y}_{\lambda_N} \\ \bar{z}_{\lambda_1} & \bar{z}_{\lambda_2} & \dots & \bar{z}_{\lambda_N} \end{bmatrix} \begin{bmatrix} \varphi_{\lambda_1} \\ \varphi_{\lambda_2} \\ \vdots \\ \varphi_{\lambda_N} \end{bmatrix}. \tag{11}$$

In Eq. (11), λ_i runs from $\lambda_1 = 360\,\text{nm}$ to $\lambda_N = 780\,\text{nm}$, and the wavelength step-size is given by the sampling interval. In the following, we adopt the usual convention of linear algebra to represent vectors by lowercase boldface letters where, e.g., $\mathbf{a}$ designates a column vector and its transpose $\mathbf{a}^t$ a row vector. With $\bar{\mathbf{x}} = [\bar{x}_{\lambda_1}, \bar{x}_{\lambda_2}, \dots, \bar{x}_{\lambda_N}]^t$, $\bar{\mathbf{y}} = [\bar{y}_{\lambda_1}, \bar{y}_{\lambda_2}, \dots, \bar{y}_{\lambda_N}]^t$, $\bar{\mathbf{z}} = [\bar{z}_{\lambda_1}, \bar{z}_{\lambda_2}, \dots, \bar{z}_{\lambda_N}]^t$, and $\boldsymbol{\varphi} = [\varphi_{\lambda_1}, \varphi_{\lambda_2}, \dots, \varphi_{\lambda_N}]^t$, Equation (11) takes the form:

$$\begin{bmatrix} X \\ Y \\ Z \end{bmatrix} = k \begin{bmatrix} \bar{\mathbf{x}}^t \\ \bar{\mathbf{y}}^t \\ \bar{\mathbf{z}}^t \end{bmatrix} \boldsymbol{\varphi}. \tag{12}$$

3.1 From Camera Channel Responses to CIE Colour Matching Functions

We now address the problem of how to approximate the $\bar{x}(\lambda), \bar{y}(\lambda), \bar{z}(\lambda)$ functions by linear combinations of the 13 spectral channels from Figure 5.

If we designate the number of individual spectral channels by M ($M = 13$ in our example), a multispectral recording of an original spectral power distribution $\boldsymbol{\varphi} = [\varphi_{\lambda_1}, \varphi_{\lambda_2}, \dots, \varphi_{\lambda_N}]^t$, will

yield M components which can be written as a vector $[C_1, C_2, \ldots, C_M]^t$:

$$\begin{bmatrix} C_1 \\ C_2 \\ \vdots \\ C_M \end{bmatrix} = \begin{bmatrix} c_{1\lambda_1} & c_{1\lambda_2} & \ldots & c_{1\lambda_N} \\ c_{2\lambda_1} & c_{2\lambda_2} & \ldots & c_{2\lambda_N} \\ \vdots & \vdots & \ddots & \vdots \\ c_{M\lambda_1} & c_{M\lambda_2} & \ldots & c_{M\lambda_N} \end{bmatrix} \begin{bmatrix} \varphi_{\lambda_1} \\ \varphi_{\lambda_2} \\ \vdots \\ \varphi_{\lambda_N} \end{bmatrix}, \tag{13}$$

where each $c_{m\lambda_n}$ represents the effective spectral sensitivity of channel m at wavelength λ_n. By designating the sampled spectral sensitivity function of channel m by a vector $\mathbf{c}_m = [c_{m\lambda_1}, c_{m\lambda_2}, \ldots, c_{m\lambda_N}]^t$, Eq. (13) reads:

$$\begin{bmatrix} C_1 \\ C_2 \\ \vdots \\ C_M \end{bmatrix} = \begin{bmatrix} \mathbf{c}_1^t \\ \mathbf{c}_2^t \\ \vdots \\ \mathbf{c}_M^t \end{bmatrix} \boldsymbol{\varphi}. \tag{14}$$

Here, the spectral sensitivities $\mathbf{c}_1, \mathbf{c}_2, \ldots, \mathbf{c}_M$ are given by the physical device characteristics of the multispectral camera.

In order to obtain a close approximation of CIE 1931 X, Y, Z values from the M channel outputs, we adopt a linear-model approach in which *approximated* values $\tilde{X}, \tilde{Y}, \tilde{Z}$ are obtained by linear combinations of the output signals C_m ($m = 1, 2, \ldots, M$) of the camera channels:

$$\begin{bmatrix} \tilde{X} \\ \tilde{Y} \\ \tilde{Z} \end{bmatrix} = \begin{bmatrix} a_{x1} & a_{x2} & \ldots & a_{xM} \\ a_{y1} & a_{y2} & \ldots & a_{yM} \\ a_{z1} & a_{z2} & \ldots & a_{zM} \end{bmatrix} \begin{bmatrix} C_1 \\ C_2 \\ \vdots \\ C_M \end{bmatrix}. \tag{15}$$

If we express the *approximated* tristimulus vector $[\tilde{X}, \tilde{Y}, \tilde{Z}]^t$ of Equation (15) in the form of Equation (12):

$$\begin{bmatrix} \tilde{X} \\ \tilde{Y} \\ \tilde{Z} \end{bmatrix} = k \begin{bmatrix} \tilde{\bar{\mathbf{x}}}^t \\ \tilde{\bar{\mathbf{y}}}^t \\ \tilde{\bar{\mathbf{z}}}^t \end{bmatrix} \boldsymbol{\varphi}, \tag{16}$$

we obtain by substituting (16) and (14) into (15):

$$k \begin{bmatrix} \tilde{\bar{\mathbf{x}}}^t \\ \tilde{\bar{\mathbf{y}}}^t \\ \tilde{\bar{\mathbf{z}}}^t \end{bmatrix} \boldsymbol{\varphi} = \begin{bmatrix} a_{x1} & a_{x2} & \ldots & a_{xM} \\ a_{y1} & a_{y2} & \ldots & a_{yM} \\ a_{z1} & a_{z2} & \ldots & a_{zM} \end{bmatrix} \begin{bmatrix} \mathbf{c}_1^t \\ \mathbf{c}_2^t \\ \vdots \\ \mathbf{c}_M^t \end{bmatrix} \boldsymbol{\varphi}. \tag{17}$$

Equation (17) is satisfied for arbitrary spectral distributions $\boldsymbol{\varphi}$ only if

$$k \begin{bmatrix} \tilde{\bar{\mathbf{x}}}^t \\ \tilde{\bar{\mathbf{y}}}^t \\ \tilde{\bar{\mathbf{z}}}^t \end{bmatrix} = \begin{bmatrix} a_{x1} & a_{x2} & \ldots & a_{xM} \\ a_{y1} & a_{y2} & \ldots & a_{yM} \\ a_{z1} & a_{z2} & \ldots & a_{zM} \end{bmatrix} \begin{bmatrix} \mathbf{c}_1^t \\ \mathbf{c}_2^t \\ \vdots \\ \mathbf{c}_M^t \end{bmatrix}. \tag{18}$$

We now have to compute the required coefficients a_{xm} ($m = 1, 2, \ldots, M$) by solving the least mean square problem

$$\sum_{\lambda_i=360\,\mathrm{nm}}^{780\,\mathrm{nm}} (\bar{x}_{\lambda_i} - \tilde{\bar{x}}_{\lambda_i})^2 = \min \tag{19}$$

and,in the same way, the coefficients a_{ym} and a_{zm} by solving

$$\sum_{\lambda_i=360\,\mathrm{nm}}^{780\,\mathrm{nm}} (\bar{y}_{\lambda_i} - \tilde{\bar{y}}_{\lambda_i})^2 = \min \tag{20}$$

and

$$\sum_{\lambda_i=360\,\mathrm{nm}}^{780\,\mathrm{nm}} (\bar{z}_{\lambda_i} - \tilde{\bar{z}}_{\lambda_i})^2 = \min \tag{21}$$

respectively. To formulate this problem more concisely, we use matrix notation with

$$\mathbf{A} = \begin{bmatrix} a_{x1} & a_{x2} & \ldots & a_{xM} \\ a_{y1} & a_{y2} & \ldots & a_{yM} \\ a_{z1} & a_{z2} & \ldots & a_{zM} \end{bmatrix}, \tag{22}$$

$$\mathbf{X} = k \begin{bmatrix} \bar{\mathbf{x}}^t \\ \bar{\mathbf{y}}^t \\ \bar{\mathbf{z}}^t \end{bmatrix} = k \begin{bmatrix} \bar{x}_{\lambda_1} & \bar{x}_{\lambda_2} & \ldots & \bar{x}_{\lambda_N} \\ \bar{y}_{\lambda_1} & \bar{y}_{\lambda_2} & \ldots & \bar{y}_{\lambda_N} \\ \bar{z}_{\lambda_1} & \bar{z}_{\lambda_2} & \ldots & \bar{z}_{\lambda_N} \end{bmatrix}, \tag{23}$$

$$\tilde{\mathbf{X}} = k \begin{bmatrix} \tilde{\bar{\mathbf{x}}}^t \\ \tilde{\bar{\mathbf{y}}}^t \\ \tilde{\bar{\mathbf{z}}}^t \end{bmatrix} = k \begin{bmatrix} \tilde{\bar{x}}_{\lambda_1} & \tilde{\bar{x}}_{\lambda_2} & \ldots & \tilde{\bar{x}}_{\lambda_N} \\ \tilde{\bar{y}}_{\lambda_1} & \tilde{\bar{y}}_{\lambda_2} & \ldots & \tilde{\bar{y}}_{\lambda_N} \\ \tilde{\bar{z}}_{\lambda_1} & \tilde{\bar{z}}_{\lambda_2} & \ldots & \tilde{\bar{z}}_{\lambda_N} \end{bmatrix}, \tag{24}$$

and

$$\mathbf{C} = \begin{bmatrix} \mathbf{c}_1^t \\ \mathbf{c}_2^t \\ \vdots \\ \mathbf{c}_M^t \end{bmatrix} = \begin{bmatrix} c_{1\lambda_1} & c_{1\lambda_2} & \ldots & c_{1\lambda_N} \\ c_{2\lambda_1} & c_{2\lambda_2} & \ldots & c_{2\lambda_N} \\ \vdots & \vdots & \ddots & \vdots \\ c_{M\lambda_1} & c_{M\lambda_2} & \ldots & c_{M\lambda_N} \end{bmatrix}. \tag{25}$$

With these designations, Equation (18) reads

$$\tilde{\mathbf{X}} = \mathbf{A}\mathbf{C} \tag{26}$$

where the matrix $\mathbf{A}$ has to be determined such that $\tilde{\mathbf{X}}$ provides a close approximation of $\mathbf{X}$. The solution of this problem is given by means of the Moore-Penrose pseudoinverse $\mathbf{C}^+$ [26, 5] of the matrix $\mathbf{C}$ as

$$\mathbf{A} = \mathbf{X}\,\mathbf{C}^+. \tag{27}$$

Figure 8 shows the results obtained by this method if the CIE 1931 colour matching functions $\bar{x}(\lambda), \bar{y}(\lambda), \bar{z}(\lambda)$ are approximated by linear combinations of the 13 spectral channels from Figure 5.

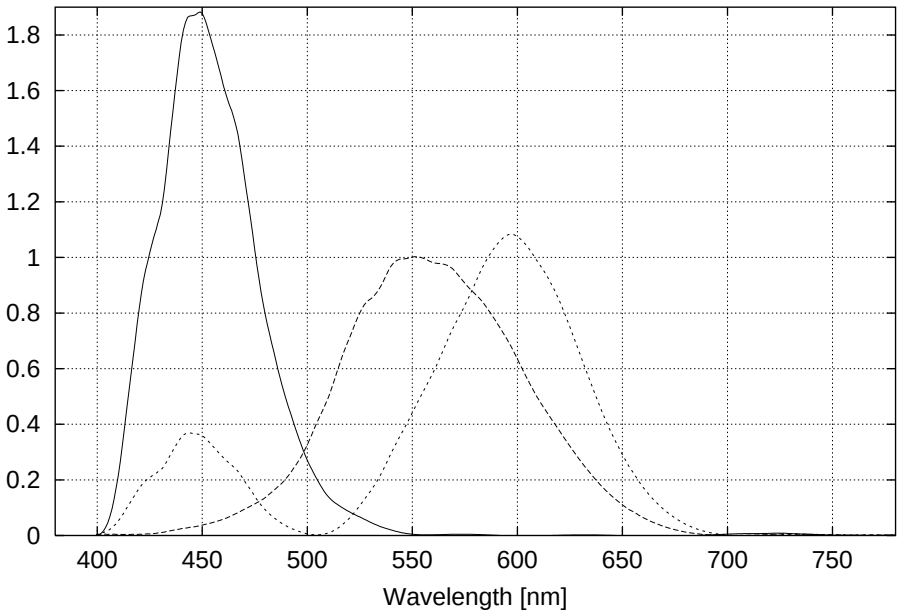

Figure 8: Approximation of the CIE 1931 XYZ colour matching functions obtained with the SpectraCam system by using linear combinations of the 13 spectral channels shown in Figure 5.

3.2 Spectral Sensitivities of an Ideal Colour Camera

In an imaging chain, a colour camera has to provide three very specific signals which depend on the primary colours of the display device. To derive the requirements for a *colorimetrically correct* imaging chain, we consider a vector $\boldsymbol{\varphi}_{ORIG}$, representing the spectral power distribution of light coming from a given position of the original scene, and a vector $\boldsymbol{\varphi}_{CRT}$ representing the spectral power distribution of the corresponding pixel on a cathode ray tube (CRT) image display.

Although $\boldsymbol{\varphi}_{ORIG}$ and $\boldsymbol{\varphi}_{CRT}$ will be generally different, they should be metamers, i.e. they should visually *match*. This is only the case if their tristimulus vectors $[X, Y, Z]^t$ as determined by Equation (12) are identical:

$$\begin{bmatrix} \bar{\mathbf{x}}^t \\ \bar{\mathbf{y}}^t \\ \bar{\mathbf{z}}^t \end{bmatrix} \boldsymbol{\varphi}_{ORIG} = \begin{bmatrix} \bar{\mathbf{x}}^t \\ \bar{\mathbf{y}}^t \\ \bar{\mathbf{z}}^t \end{bmatrix} \boldsymbol{\varphi}_{CRT}. \tag{28}$$

Since the light output $\boldsymbol{\varphi}_{CRT}$ of the CRT display is the result of additive colour mixing, it can be expressed as:

$$\boldsymbol{\varphi}_{CRT} = R\,\boldsymbol{\varphi}_{CRT\,R} + G\,\boldsymbol{\varphi}_{CRT\,G} + B\,\boldsymbol{\varphi}_{CRT\,B}, \tag{29}$$

where $\boldsymbol{\varphi}_{CRT\,R}$, $\boldsymbol{\varphi}_{CRT\,G}$, and $\boldsymbol{\varphi}_{CRT\,B}$ designate the spectral power distributions of the CRT-primaries. The coefficients R, G, B are weighting factors which determine the relative contribution of each primary to the total light output $\boldsymbol{\varphi}_{CRT}$ of the display. The values of R, G, B are between 0 and 1, these limits being reached for none and full contributions respectively. Note that the R, G, B

coefficients represent light quantities rather than video signal amplitudes; because of the nonlinear relationship between video signals and CRT light output, they are linked to the video signal values by a nonlinear function, commonly referred to by a power function with an exponent called γ $(gamma)$.

Using the notations of linear algebra, Eq. (29) can be rewritten as the product of the N-row $\times$ 3-column matrix formed by the three primary vectors $[\boldsymbol{\varphi}_{CRT\,R},\ \boldsymbol{\varphi}_{CRT\,G},\ \boldsymbol{\varphi}_{CRT\,B}]$ with a column vector containing the coefficients R, G, B:

$$\boldsymbol{\varphi}_{CRT} = [\boldsymbol{\varphi}_{CRT\,R},\ \boldsymbol{\varphi}_{CRT\,G},\ \boldsymbol{\varphi}_{CRT\,B}] \begin{bmatrix} R \\ G \\ B \end{bmatrix}. \tag{30}$$

By substituting $\boldsymbol{\varphi}_{CRT}$ from Eq. (30) in Eq. (28), we get

$$\begin{bmatrix} \bar{\mathbf{x}}^t \\ \bar{\mathbf{y}}^t \\ \bar{\mathbf{z}}^t \end{bmatrix} \boldsymbol{\varphi}_{ORIG} = \begin{bmatrix} \bar{\mathbf{x}}^t \\ \bar{\mathbf{y}}^t \\ \bar{\mathbf{z}}^t \end{bmatrix} [\boldsymbol{\varphi}_{CRT\,R},\ \boldsymbol{\varphi}_{CRT\,G},\ \boldsymbol{\varphi}_{CRT\,B}] \begin{bmatrix} R \\ G \\ B \end{bmatrix}. \tag{31}$$

We can now use Eq. (12) to replace the matrix product on the right side of Eq. (31) by a 3×3 matrix which contains the CIEXYZ tristimulus values of the CRT phosphors:

$$\begin{bmatrix} \bar{\mathbf{x}}^t \\ \bar{\mathbf{y}}^t \\ \bar{\mathbf{z}}^t \end{bmatrix} \boldsymbol{\varphi}_{ORIG} = \frac{1}{k} \begin{bmatrix} X_R & X_G & X_B \\ Y_R & Y_G & Y_B \\ Z_R & Z_G & Z_B \end{bmatrix} \begin{bmatrix} R \\ G \\ B \end{bmatrix}. \tag{32}$$

Finally, the solution of Eq. (32) for $[R, G, B]^t$ reads:

$$\begin{bmatrix} R \\ G \\ B \end{bmatrix} = k \begin{bmatrix} X_R & X_G & X_B \\ Y_R & Y_G & Y_B \\ Z_R & Z_G & Z_B \end{bmatrix}^{-1} \begin{bmatrix} \bar{\mathbf{x}}^t \\ \bar{\mathbf{y}}^t \\ \bar{\mathbf{z}}^t \end{bmatrix} \boldsymbol{\varphi}_{ORIG} \tag{33}$$

Equation (33) tells us how to obtain the colorimetrically correct CRT-primary contributions R, G, B for any colour stimulus given by its spectral power distribution $\boldsymbol{\varphi}_{ORIG}$. An ideal colorimetric camera, providing directly the R, G, B coefficients, would have to implement spectral sensitivities $\mathbf{c}_R, \mathbf{c}_G, \mathbf{c}_B$ such that

$$\begin{bmatrix} R \\ G \\ B \end{bmatrix} = \begin{bmatrix} \mathbf{c}_R^t \\ \mathbf{c}_G^t \\ \mathbf{c}_B^t \end{bmatrix} \boldsymbol{\varphi}_{ORIG} \tag{34}$$

for any $\boldsymbol{\varphi}_{ORIG}$. According to Equation (33), we get

$$\begin{bmatrix} \mathbf{c}_R^t \\ \mathbf{c}_G^t \\ \mathbf{c}_B^t \end{bmatrix} = k \begin{bmatrix} X_R & X_G & X_B \\ Y_R & Y_G & Y_B \\ Z_R & Z_G & Z_B \end{bmatrix}^{-1} \begin{bmatrix} \bar{\mathbf{x}}^t \\ \bar{\mathbf{y}}^t \\ \bar{\mathbf{z}}^t \end{bmatrix}. \tag{35}$$

In other words, the requirement (28) can be satisfied for any $\boldsymbol{\varphi}_{ORIG}$ if and only if the spectral sensitivity functions of each of the camera's three colour channels are linear combinations of the colour matching functions of the human observer.

Table 1: CIE 1931 chromaticities for ITU-R BT.709 reference primaries and CIE standard illuminant D65.

	Red $R\,709$	Green $G\,709$	Blue $B\,709$	White D65
x	0.6400	0.3000	0.1500	0.3127
y	0.3300	0.6000	0.0600	0.3290
z	0.0300	0.1000	0.7900	0.3583

3.3 Implementation of an Ideal Colour Camera for ITU-R BT.709 CRT-primaries

In section 3.1 we showed how to obtain CIE 1931 X, Y, Z colorimetric values from the output signals of a multispectral camera. Another interesting application of interactive multispectral image acquisition is the implementation of the spectral sensitivity functions of the blue, green, and red colour channels of an ideal colour camera for a display using ITU-R BT.709 or sRGB primaries [10, 11].

The spectral sensitivity functions $\mathbf{c}_{R\,709}, \mathbf{c}_{G\,709}, \mathbf{c}_{B\,709}$ of such an ideal camera are directly obtained from Equation (35) if we use the CIEXYZ tristimulus values of the ITU-R BT.709 primaries in the 3×3 matrix:

$$\begin{bmatrix} \mathbf{c}^t_{R709} \\ \mathbf{c}^t_{G709} \\ \mathbf{c}^t_{B709} \end{bmatrix} = k \begin{bmatrix} X_{R\,709} & X_{G\,709} & X_{B\,709} \\ Y_{R\,709} & Y_{G\,709} & Y_{B\,709} \\ Z_{R\,709} & Z_{G\,709} & Z_{B\,709} \end{bmatrix}^{-1} \begin{bmatrix} \bar{\mathbf{x}}^t \\ \bar{\mathbf{y}}^t \\ \bar{\mathbf{z}}^t \end{bmatrix}. \tag{36}$$

The only remaining question is how to obtain the CIEXYZ values for the 3×3 matrix in Equation (36) from the chromaticity coordinates of the ITU-R BT.709 reference primaries and of the CIE standard illuminant D65, given in table 1.

From the general definition of the chromaticies x, y, z

$$\begin{aligned} x &= \frac{X}{X+Y+Z} \\ y &= \frac{Y}{X+Y+Z} \\ z &= \frac{Z}{X+Y+Z} \end{aligned} \tag{37}$$

follows, for any colour stimulus i,

$$\begin{bmatrix} X_i \\ Y_i \\ Z_i \end{bmatrix} = \begin{bmatrix} x_i \\ y_i \\ z_i \end{bmatrix} m_i \tag{38}$$

with

$$m_i = X_i + Y_i + Z_i \tag{39}$$

On an ideal ITU-R BT.709 display device, equal 100% video signals on all three video inputs should produce a white stimulus with D65 chromaticity. In terms of CIE 1931 tristimulus vector components, this additive mixing can be expressed as:

$$\begin{bmatrix} X_{D65} \\ Y_{D65} \\ Z_{D65} \end{bmatrix} = \begin{bmatrix} X_{R\,709} \\ Y_{R\,709} \\ Z_{R\,709} \end{bmatrix} + \begin{bmatrix} X_{G\,709} \\ Y_{G\,709} \\ Z_{G\,709} \end{bmatrix} + \begin{bmatrix} X_{B\,709} \\ Y_{B\,709} \\ Z_{B\,709} \end{bmatrix}. \tag{40}$$

By substituting (38) for $i = R\,709, G\,709, B\,709, D65$, into (40), we get

$$\begin{bmatrix} x_{D65} \\ y_{D65} \\ z_{D65} \end{bmatrix} m_{D65} = \begin{bmatrix} x_{R\,709} \\ y_{R\,709} \\ z_{R\,709} \end{bmatrix} m_{R\,709} + \begin{bmatrix} x_{G\,709} \\ y_{G\,709} \\ z_{G\,709} \end{bmatrix} m_{G\,709} + \begin{bmatrix} x_{B\,709} \\ y_{B\,709} \\ z_{B\,709} \end{bmatrix} m_{B\,709} \tag{41}$$

which reads in Matrix notation

$$\begin{bmatrix} x_{D65} \\ y_{D65} \\ z_{D65} \end{bmatrix} m_{D65} = \begin{bmatrix} x_{R\,709} & x_{G\,709} & x_{B\,709} \\ y_{R\,709} & y_{G\,709} & y_{B\,709} \\ z_{R\,709} & z_{G\,709} & z_{B\,709} \end{bmatrix} \begin{bmatrix} m_{R\,709} \\ m_{G\,709} \\ m_{B\,709} \end{bmatrix}. \tag{42}$$

The solution of Equation (42) is given by

$$\begin{bmatrix} m_{R\,709} \\ m_{G\,709} \\ m_{B\,709} \end{bmatrix} = \begin{bmatrix} x_{R\,709} & x_{G\,709} & x_{B\,709} \\ y_{R\,709} & y_{G\,709} & y_{B\,709} \\ z_{R\,709} & z_{G\,709} & z_{B\,709} \end{bmatrix}^{-1} \begin{bmatrix} x_{D65} \\ y_{D65} \\ z_{D65} \end{bmatrix} m_{D65} \tag{43}$$

where the only still unknown quantity is m_{D65}. To determine m_{D65}, we take the center line of Equation (38) for $i = D65$:

$$Y_{D65} = y_{D65}\, m_{D65}. \tag{44}$$

Here, Y_{D65} represents the luminance of the nominal white stimulus as determined by a photometric measurement, and m_{D65} in Equation (43) therefore can be replaced by

$$m_{D65} = Y_{D65}/y_{D65}. \tag{45}$$

Equation (43) is now completely determined, and we can use the resulting values $m_{R\,709}, m_{G\,709}, m_{B\,709}$ to compute the CIEXYZ values of the ITU-R BT.709 primaries according to Equation (38):

$$\begin{bmatrix} X_{R\,709} & X_{G\,709} & X_{B\,709} \\ Y_{R\,709} & Y_{G\,709} & Y_{B\,709} \\ Z_{R\,709} & Z_{G\,709} & Z_{B\,709} \end{bmatrix} = \begin{bmatrix} x_{R\,709} & x_{G\,709} & x_{B\,709} \\ y_{R\,709} & y_{G\,709} & y_{B\,709} \\ z_{R\,709} & z_{G\,709} & z_{B\,709} \end{bmatrix} \begin{bmatrix} m_{R\,709} & 0 & 0 \\ 0 & m_{G\,709} & 0 \\ 0 & 0 & m_{B\,709} \end{bmatrix}. \tag{46}$$

Figure 9 shows the resulting spectral sensitivity functions $\mathbf{c}_{R\,709}, \mathbf{c}_{G\,709}, \mathbf{c}_{B\,709}$ of an ideal camera for ITU-R BT.709 primaries obtained by substituting the matrix of the CIEXYZ values (46) into Equation (36).

To implement these ITU-R BT.709 spectral sensitivity functions on our interactive multispectral camera system, we used again linear combinations of the 13 spectral channels from Figure 5. The procedure is exactly the same as described in Section 3.1 and the results are shown in Figure 10.

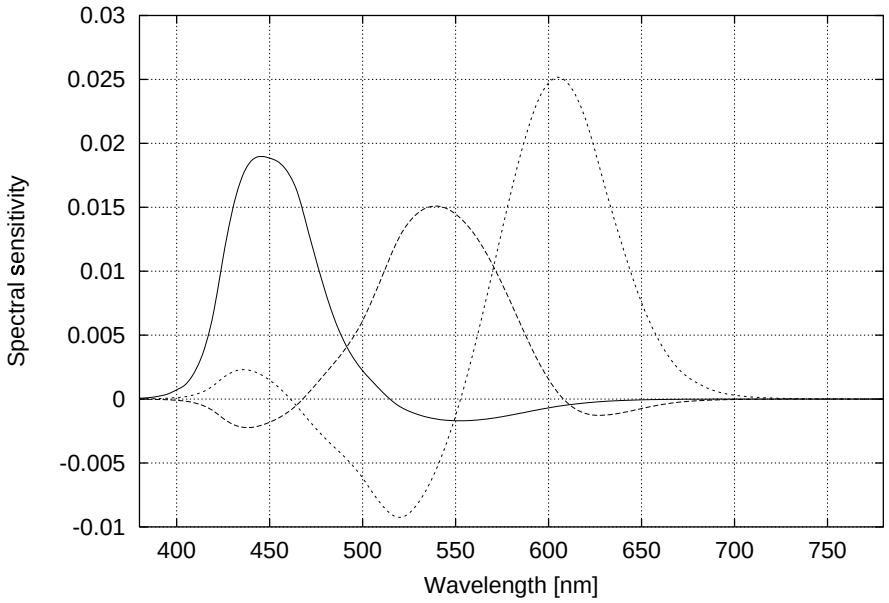

Figure 9: Theoretically correct spectral sensitivity functions of the blue, green, and red colour channels of an ideal colour camera for a display using ITU-R BT.709 or sRGB primaries.

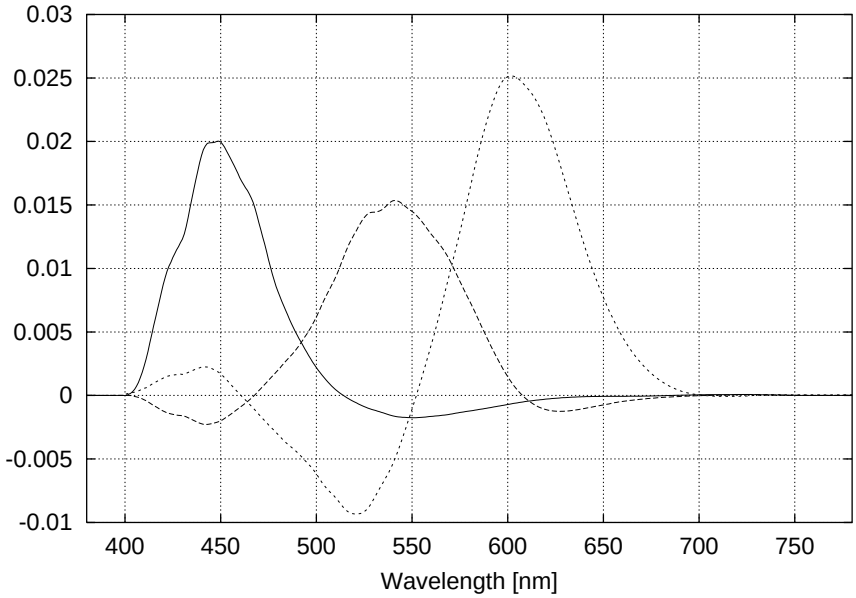

Figure 10: Approximation by our SpectraCam system of the spectral sensitivity functions of an 'ideal' colour camera for a display using ITU-R BR.709 primaries. This approximation is obtained by using linear combinations of the 13 spectral channels shown in Figure 5.

4 Conclusion

This paper presents a fully electronic system for multispectral image acquisition and analysis which allows for interactive operation across the Web.

The key elements of the system are an electronically controlled liquid crystal tunable filter, a digital camera, and modular software components based on a client-server architecture. On the server side, Java Servlets are used to implement access to the system through simple HTTP requests. Since only the standard Common Gateway Interface (CGI) mechanisms for client-server communication are used, the system is accessible from any Web browser.

In its present form, the system provides realtime remote access on our intranet to reflectance spectra at any position on the target. The user typically first selects the reference 'white' position by means of the mouse cursor, and then interactively examines reflectance spectra, CIE XYZ tristimulus values, or CIELab data for any region of interest. Application areas include the spectrophotometric analysis of fine art paintings and museum objects, the simulation of object appearance under different illuminants, and high-end multimedia colour imaging.

References

[1] Brian A. Wandell. The synthesis and analysis of color images. *IEEE Transactions on Pattern Analysis and Machine Intelligence* **9,** 2–13, (1987).

[2] Joyce E. Farell. Spectral based color image editing (SBCIE). In *Proceedings of IS&T and SID's 4th Color Imaging Conference: Color Science, Systems and Applications*, pg. 104–108, Scottsdale, Arizona, (1996).

[3] Henri Maître, Francis Schmitt, Jean-Pierre Crettez, Yifeng Wu, and Jon Yngve Hardeberg. Spectrophotometric image analysis of fine art paintings. In *Proceedings of IS&T and SID's 4th Color Imaging Conference: Color Science, Systems and Applications*, pg. 50–53, Scottsdale, Arizona, (1996).

[4] Roy S. Berns, Francisco H. Imai, Peter D. Burns, and Di-Y. Tzeng. Multi-spectral-based color reproduction research at the Munsell Color Science Laboratory. In *Electronic Imaging: Processing, Printing, and Publishing in Color*, pg. 14–25, SPIE Vol. 3409, (1998).

[5] Jon Yngve Hardeberg, Francis Schmitt, Hans Brettel, Jean-Pierre Crettez, and Henri Maître. Multispectral image acquisition and simulation of illuminant changes. In L. W. MacDonald and M. R. Luo, editors, *Colour Imaging: Vision and Technology*, pg. 145–164. Wiley, 1999.

[6] Friedhelm König and Werner Praefcke. The practice of multispectral image acquisition. In *Electronic Imaging: Processing, Printing, and Publishing in Color*, pg. 34–41, SPIE Vol. 3409, (1998).

[7] Wencheng Wu, Jan P. Allebach, and Mostafa Analoui. Imaging colorimetry using a digital camera. In *Proceedings of IS&T and SID's 7th Color Imaging Conference: Color Science, Systems and Applications*, pg. 15–20, Scottsdale, Arizona, (1999).

[8] CIE. *Colorimetry. Publ. CIE No. 15.2.* Commission Internationale d'Eclairage, Vienna, 1986.

[9] CIE. *CIE Standard Colorimetric Observers. Publ. CIE No. S002.* Commission Internationale d'Eclairage, Vienna, 1986.

[10] Recommendation ITU-R BT.709-3. Parameter values for the HDTV standards for production and international programme exchange. International Telecommunication Union, Geneva, 1997.

[11] M. Stokes, M. Anderson, S. Chandrasekar, and R. Motta. A standard default color space for the Internet - sRGB. `http://www.w3.org/Graphics/Color/sRGB.html`, 1996.

[12] P. H. Swain and S. M. Davis, editors. *Remote Sensing: The Quantitative Approach.* McGraw-Hill, New York, 1978.

[13] Armel Rosselet, Werner Graff, Urs P. Wild, C. U. Keller, and Rudolf Gschwind. Persistent spectral hole burning used for spectrally high-resolved imaging of the sun. In *Imaging Spectrometry*, volume 2480 of *SPIE Proceedings*, pg. 205–212, 1995.

[14] Hideaki Haneishi, T. Hasegawa, Norimichi Tsumura, and Yoichi Miyake. Design of color filters for recording art works. In *Proceedings of IS&T 50th Annual Conference*, pg. 369–372, 1997.

[15] D. L. Farkas, B. T. Ballou, G. W. Fisher, D. Fishman, Y. Garini, W. Niu, and E. S. Wachman. Microscopic and mesoscopic spectral bio-imaging. In *Proc. Soc. Photo-Optical Instr. Eng*, volume 2678, pg. 200–206, 1996.

[16] Roy S. Berns. Challenges for color science in multimedia imaging. In *Conference Proceedings, CIM'98, Colour Imaging in Multimedia*, pg. 123–133, Derby, UK, (1998).

[17] Mark S. Peercy. Linear color representations for full spectral rendering. *Computer Graphics Proceedings* **,** 191–198, 1993.

[18] Bernard Lyot. Un monochromateur à grand champ utilisant les interférences en lumière polarisée. *Comptes Rendus de l'Académie des Sciences* **197,** 1593–1595, 1933.

[19] Tom Chrien, Chris Chovit, and Peter Miller. Imaging spectrometry using liquid crystal tunable filters. `http://stargate.jpl.nasa.gov/lctf/rtf/`, 1993.

[20] W3C. HTTP - hypertext transfer protocol overview. `http://www.w3.org/Protocols/`.

[21] W3C. HTML - hypertext markup language. `http://www.w3.org/MarkUp/`.

[22] Sun Microsystems. The java tutorial: Overview of the jni. `http://java.sun.com/docs/books/tutorial/native1.1/concepts/index.html`, 1999.

[23] Sun Microsystems. The java communications api. `http://www.javasoft.com/products/javacomm/`.

[24] The MathWorks and National Institute of Standards and Technology (NIST). Jama: A java matrix package. `http://math.nist.gov/javanumerics/jama`, 1998.

[25] G. Wyszecki and W. S. Stiles. *Color Science.* Wiley, New York, 2nd edition, 1982.

[26] A. Albert. *Regression and the Moore-Penrose pseudoinverse.* Academic Press, 1972.